Urban Park Vegetation Indices and Local Cooling in Krakow: A Linear Mixed Effects Model Analysis of Landsat Land Surface Temperature

Ewa Głowienka, *Member, IEEE, and* Marcin Kucza, *Fellow, IEEE*

***Abstract*— Park cooling in Krakow was quantified with archival Landsat imagery from 1990, 2000, 2013, and 2018. A linear mixed effects model with random intercepts for Area and PointID was applied to 33,949 locations and about 136,000 samples. Land surface temperature (LST) was retrieved with Landsat Collection 2 Level-2 Surface Temperature product. Cooling was defined as the within scene difference in LST between park cores at 0 m and fixed buffers at 150 and 300 m. NDVI and NDMI were included as standardized predictors. Between 1990 and 2018, mean LST rose by about 4 °C. Park cores were cooler than the 150 m buffer by about ~2.1–2.6°C, and cooler than the 300 m buffer by about ~2.6–3.3°C. The distance decay changed over time. The core to edge contrast peaked around 2000. Relative to 1990, the contrast in 2000 was larger by 0.50 °C at 150 m and by 0.67 °C at 300 m. It weakened by 2013 and partly recovered in 2018. NDMI showed a stronger association with LST than NDVI (−1.25°C per one standard deviation; p < 0.001 versus NDVI non-significant (p=0.846)). Fixed effects explained about 37.5% of variance and the full model about 95.6%. The results show persistent mitigation of surface heat by urban forests and point to the importance of canopy moisture and the protection of near park buffers. The study provides reference values that can be compared across cities and years to guide evaluation of urban heat mitigation.**

***Index Terms*— land surface temperature; urban heat island; park cool island; NDMI; Landsat; mixed effects model**

This work was supported in part by the "Excellence initiative – research university" program at AGH University of Krakow. *(Corresponding author: Ewa Głowienka)*

Ewa Głowienka and Marcin Kucza are with the Faculty of Geo-Data Science, Geodesy, and Environmental Engineering, AGH University of Krakow, 30-059 Krakow, Poland (e-mail: eglo@agh.edu.pl; mkucza@agh.edu.pl).

I. INTRODUCTION

CITIES worldwide are experiencing unprecedented warming as urbanization and climate change drive up temperatures. In dense urban areas, the well-known urban heat island (UHI) effect exacerbates heat extremes by trapping heat in built surfaces and reducing nighttime cooling [1], [2]. The UHI leads to higher day- and nighttime temperatures in cities relative to rural surroundings, intensifying heat stress, raising building cooling demands, and impacting public health [2]. Accordingly, there is a critical need to monitor and understand urban thermal environments over time. Satellite remote sensing provides a powerful tool in this regard: thermal infrared sensors on platforms like Landsat and MODIS can continuously map land surface temperature (LST) across entire cities and over long periods[3], [4]. Such observations enable consistent long-term analysis of surface heat patterns and UHI intensity at fine spatial resolutions that are not feasible with sparse ground measurements [5], [6]. Over the past decades, these techniques have revealed strong links between urban development, vegetation loss, and rising surface temperatures in cities worldwide [7], [8].

Urban green infrastructure has emerged as an essential strategy for mitigating urban heat [9], [10]. Trees, parks, and other vegetated spaces cool their surroundings through shading of solar radiation and evapotranspiration of water, which dissipates heat as latent energy [2], [10]. These cooling ecosystem services give rise to the so-called "park cool island" (PCI) effect, wherein urban parks maintain lower surface temperatures than the surrounding built-up neighborhoods [11], [12]. A wide range of empirical studies have documented PCI effects in cities of varying climates. For example, a meta-analysis found that urban green areas are generally about 1 °C cooler on average (with up to a few degrees difference in some cases) compared to non-vegetated urban patches [11], [13]. Case studies in arid, tropical, and temperate cities likewise report daytime park cooling on the order of 1–5 °C, depending on park size and conditions [14], [15].

Park cooling can also extend beyond park boundaries: temperature reductions have been observed up to roughly a few hundred meters into the surrounding urban area [11], [13], [16]. However, the magnitude and spatial reach of a PCI vary with local factors. Larger parks with abundant tree cover tend to generate stronger and more enduring cool islands than smaller or sparsely vegetated parks [13], [17], while even small pocket parks or street tree clusters can provide measurable micro-scale cooling benefits [18], [19]. Vegetation type is also important: tree-covered areas produce substantially greater cooling than those with only low grass or shrubs [20]. The presence of open water bodies (e.g., lakes) can further amplify a park's cooling effect [21]. Climate setting plays a role as well: cities in humid or temperate climates often exhibit a more pronounced vegetation cooling effect than those in hot, arid regions, where limited moisture and higher ambient heat constrain evapotranspirative cooling [22], [23], [24]. Beyond park size

and canopy composition, the degree of forest fragmentation can influence both the magnitude and spatial footprint of cooling. Fragmentation reduces core area and increases edge exposure, which can diminish canopy moisture and evapotranspiration, thereby weakening surface cooling and altering the PCI gradient. Recent satellite analyses report asymmetric thermal responses to forest cover gain versus loss [25] and warming feedbacks from forest degradation [26].

Despite significant progress in characterizing park cool islands, important research gaps remain. Most remote sensing studies of urban vegetation and LST to date have been cross-sectional, examining a single city or a single time period [5]. Relatively few have investigated how the cooling effect of urban parks evolves over multiple decades as cities grow and climates warm. Long-term analyses are needed to determine whether green-space cooling benefits persist or diminish over time under urban expansion and global warming. A recent global analysis confirmed that urban parks are on average about 1.5 °C cooler than their surroundings [27], but such broad studies provide only a snapshot and do not capture temporal trends.

In addition, prior remote sensing assessments have predominantly relied on vegetation indices like the Normalized Difference Vegetation Index (NDVI) as proxies for plant cover and health [5], [28]. NDVI is a convenient indicator of greenness that generally correlates inversely with LST – areas with higher NDVI tend to exhibit lower surface temperatures [8], [29]. However, greenness alone may not fully capture the cooling capacity of urban vegetation, since plant water content and soil moisture also play critical roles in evapotranspiration cooling [22], [24], [30]. An index that accounts for moisture, such as the Normalized Difference Moisture Index (NDMI), could potentially serve as a stronger predictor of park cooling by reflecting water availability for latent heat flux. To date, the relative importance of canopy greenness versus moisture for urban temperature mitigation remains underexplored; few studies have explicitly compared NDVI and NDMI (or related moisture indices) in their relationship to LST [5]. A further limitation in the literature is the inconsistent definition of what constitutes an "urban park" and its buffer, which complicates cross-city comparisons. Different researchers have delineated park boundaries and surrounding zones in varying ways, from simple distance buffers to subjective neighborhood extents. Standardized spatial frameworks, such as the European Urban Atlas land-use polygons [31], [32] or the Local Climate Zone scheme [1], have not yet been widely applied to PCI studies, but offer a means to make results more comparable across cities.

These knowledge gaps are addressed by analyzing the long-term LST trends associated with major urban green spaces in Krakow, where urban expansion and redevelopment in recent decades have raised concerns about rising heat exposure [33]. Specifically, the research questions are: (1) Did the parks in Krakow remain significantly cooler than their urban surroundings throughout 1990–2018, and how did the magnitude of this cooling differential change over time? (2) Have city-wide surface temperatures increased significantly over the study period? (3) To what extent do vegetation indices (NDVI, NDMI) explain the spatio-temporal variability in LST, and does NDMI provide additional explanatory power for LST beyond NDVI? It was hypothesized that the interior of each park would exhibit significantly lower LST than the surrounding built-up areas in all years, reflecting a persistent PCI effect. LST was also expected to be inversely related to vegetation index values, with NDMI showing a stronger cooling influence than NDVI. Finally, daytime late spring (May) LST in the study area was anticipated to have increased from 1990 to 2018, in line with broader warming trends.

A multi-year assessment (1990–2018) of the park cool island in a Central European city is presented using a linear mixed model [34], [35], [36], [37]. The approach quantifies, in degrees Celsius, the contributions of canopy moisture (NDMI) and greenness (NDVI) [38], [39] to reducing land surface temperature, enabling a direct comparison of their effects [29], [30], [40]. This study provides a rare longitudinal view of park-related surface cooling while explicitly contrasting moisture- and greenness-based predictors within one statistical framework — linear mixed effects model (LMM).

To test these hypotheses and quantify the influence of vegetation on urban LST, a linear mixed effects model was fitted with random intercepts for Area and PointID. Predictors included Year (1990, 2000, 2013, 2018), Zone (0 m, 150 m, 300 m), NDVI, and NDMI. This modeling framework accounts for variability across different urban contexts through random effects, ensuring robust and generalizable estimates of the vegetation–temperature relationships. The model translates changes in NDVI and NDMI into absolute temperature reductions (°C), allowing direct quantification of the cooling effect attributable to vegetation. This approach provides clear, quantitative evidence of temperature reduction due to urban greening, effectively expressing heat-mitigation benefits in physical temperature units. The findings underscore the model's utility for urban climate analysis and provide practical information for spatial planning aimed at climate change adaptation.

II. Materials and Methods

A. Study area

Krakow is a city located in Poland, Central Europe (population ~770,000) with a temperate climate. The terrain is moderately varied, with elevations ranging from ~188 m above sea level in the Vistula valley to over 350 m in the surrounding hills. The topography, together with the prevailing westerly winds, influences local ventilation patterns and thermal conditions. This region provides a useful field for analyzing three decades of surface UHI dynamics in the vicinity of clearly defined green areas consisting of forests and a historic downtown park. Previous studies in this area have documented distinct spatial patterns of LST and summer hot spots using Landsat thermal data [33].

Four main green areas were selected for analysis (Fig. 1), representing both extensive suburban forests and an inner-city park:

- Wolski Forest (Las Wolski) – a large (~419 ha)

complex of mixed deciduous and coniferous forests on the western fringes of Krakow, dominated by oak (Quercus robur), beech (Fagus sylvatica) and pine (Pinus sylvestris).

- Legowski Forest (Las Łęgowski) – a small riparian mixed forest (~24 ha) in the northern part of the city, containing black alder (Alnus glutinosa) stands and periodically flooded habitats.
- Zabierzowski Forest (Las Zabierzowski) – a forest covering an area of approximately 387 ha located northwest of the city, featuring hornbeam and oak communities and fragments of pine plantations.
- Planty Park (Planty) – a park of approximately 21 hectares surrounding the Old Town, planted with a mixture of deciduous tree species and serving as a "green ring" in the densely built-up city center.

Park extents and buffers (0, 150, 300 m) were delineated from the standardized Copernicus Urban Atlas 2018 polygons (Fig.1b) and kept fixed across all epochs, to ensure spatial comparability [31]. For context and nomenclature consistency, we also used CORINE Land Cover 2018 [32] and cross-walked equivalent classes to harmonize definitions of green areas (e.g., CLC 141 ↔ UA 14100; CLC 142 ↔ UA 14200). These buffer distances encompass the range of typical PCI extents reported in the literature (on order of 100–300 m from the green space edge) [11], [12], [13], [14], [15], [16]. The buffers intersect a variety of surrounding land uses — from high-density built-up areas in the case of Planty, to low-density residential and agricultural lands around the peri-urban forests—providing a gradient of urbanization for analysis. Park boundaries and 0/150/300 m buffers were kept fixed across all years to ensure spatial comparability. NDVI and NDMI were computed for each epoch and used as pixel level covariates to represent vegetation amount and moisture across the heterogeneous surfaces within parks and buffers. Land cover transitions within the fixed buffers, including changes in impervious and built surfaces, are not represented explicitly and are treated as a source of uncertainty in the interpretation of long term PCI changes (Section IV.D). Because the Planty site is located in the dense historic core, the 150–300 m ring contains no pixels mapped as vegetation in the Copernicus Urban Atlas (UA2018) classes; consequently, the 300 m ring was not included in the buffer-based NDVI/NDMI summaries (Fig. 1 C). Park Planty was analysed only for the 0 m and 150 m zones in the zone summaries and in the mixed model.

Within each zone (interior 0 m, 150 m, 300 m), the complete set of 30 m cell centroids was used as point locations. The same grid was retained in all years. Each point record stores coordinates (X, Y), site (Area), zone, and year. Zones do not overlap. In total, the dataset contains approximately 135,794 records for approximately 33,949 unique PointIDs observed in 1990, 2000, 2013, and 2018. This design preserves exact spatial comparability across years and allows modeling of repeated measurements at the same 30 m location. The spatial distribution of point locations by park and zone is provided in Supplementary Fig. S5.

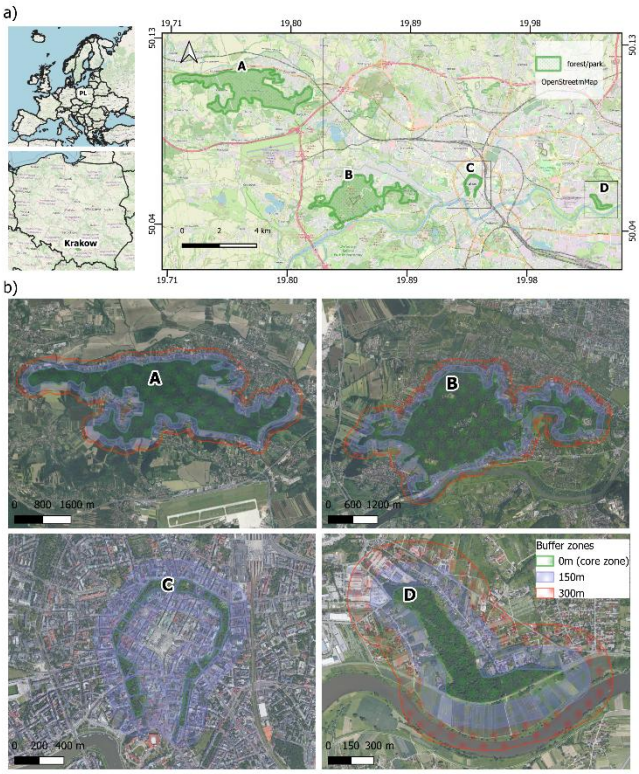

Fig. 1. Study area and park buffer zones. (a) Regional location of Krakow, Poland, and the four analyzed green areas (A–D). (b) Detailed views of each site showing park extents (from Copernicus Urban Atlas 2018) and the fixed buffer zones used in the analysis: 0 m (core), 150 m, and 300 m. A — Zabierzowski Forest; B — Wolski Forest; C — Planty Park; D — Legowski Forest. For (C) Planty, the 300 m ring is not included in zone summaries and in the mixed model because the 150–300 m zone contains no pixels mapped as vegetation. All analyses were conducted in WGS 84 / UTM zone 34N (EPSG: 32634).

B. Data

The dataset summarized in Table I was used to compute NDVI and NDMI and to derive land surface temperature (LST) for four epochs (1990, 2000, 2013, 2018). USGS Landsat Collection 2 products were used: surface reflectance for optical bands and the Level-2 Surface Temperature product for LST [41], [42]. Scenes were filtered using the QA metadata, and per-pixel masks for cloud, shadow, snow/ice, and water were applied. All rasters were coregistered to a common WGS 84 / UTM Zone 34N grid (EPSG: 32634) and resampled to 30 m; continuous variables were resampled with bilinear interpolation and categorical masks with nearest neighbor. For Landsat 8 TIRS, only Band 10 was used, following USGS guidance [42]. Radiometric consistency across sensors and dates follows Collection 2 specifications, ensuring comparability of reflectance and LST inputs [41], [42].

The four years were chosen because each provides a cloud-free Landsat scene during peak vegetation in late spring. The 2012 season was avoided due to the Landsat-7 scan line corrector failure, and 2013 uses Landsat-8 OLI/TIRS [41], [42]. All four

scenes share comparable clear sky, late spring conditions (Table I). Together with standardized park boundaries from Copernicus UA/CLC and fixed buffers across decades (Section II-A), these choices provide a consistent basis for comparison among sensors and years and support interpreting the ~4 °C warming and the changing contrast between parks and their surroundings as decadal change rather than a single day anomaly.

TABLE I
SATELLITE DATA - DATE AND TIME

Satellite WRS-2 Path/Row	**Date (yyyy-mm-dd)**	**UTC time (hh:mm:ss)**	**Scene ID (LANDSAT_ID)**
Landsat 5 188/25	1990-05-04	8:52:35	LT05_188025_19900504
	2000-05-15	9:08:13	LT05_188025_20000515
Landsat 8 188/25	2013-05-19	9:34:27	LC08_188025_20130519
	2018-05-01	9:31:37	LC08_188025_20180501

All four scenes are clear sky May acquisitions at comparable late-morning local time overpasses (~10:50–11:35 LT) and were processed with QA-based cloud/shadow masking and co-registered to a common UTM grid. This ensures phenologically comparable and radiometrically stable conditions across years, thereby mitigating short-term weather fluctuations and seasonal shifts. As a result, inter-annual differences reported here primarily reflect long term signals rather than day-to-day meteorology.

C. Spectral Indices Calculation

NDVI and NDMI were computed from surface reflectance as follows [38], [39]:

$$NDVI = \frac{NIR - Red}{NIR + Red} \quad (1)$$

$$NDMI = \frac{NIR - SWIR1}{NIR + SWIR1} \quad (2)$$

Where:
NIR — surface reflectance in the near-infrared band (Landsat 5: B4; Landsat 8: B5).
Red — surface reflectance in the red band (Landsat 5: B3; Landsat 8: B4).
SWIR1 — surface reflectance in short-wave infrared band 1 (Landsat 5: B5; Landsat 8: B6).

NDVI is a long-established proxy of canopy greenness and density [16], [33], [38]. NDMI (sometimes referred to as a moisture sensitive normalized difference water index) emphasizes liquid water content in vegetation and soils and has been widely used as a proxy for canopy moisture in forest studies [38], [39].

D. Land Surface Temperature Retrieval

Land surface temperature was obtained from the USGS Landsat Collection 2 Level 2 Surface Temperature product for each acquisition [41], [42]. The product provides per pixel surface temperature together with QA layers, and it includes an operational atmospheric correction and emissivity estimate used in the retrieval. Digital numbers in the surface temperature band were first converted to physical temperature using the published scale factor and add offset, and then expressed in degrees Celsius. Pixels flagged as cloud, cloud shadow, snow or ice, water, or invalid temperature were excluded using the Level 2 QA layers before sampling. Although the surface temperature product is distributed on a 30 m grid, the thermal information originates from the native thermal sampling (120 m for Landsat 5 TM and 100 m for Landsat 8 TIRS). For spatial alignment with the surface reflectance bands used to compute NDVI and NDMI, continuous rasters were resampled with bilinear interpolation, while categorical masks were resampled with nearest neighbour. The analysis focuses on within scene contrasts between the park interior and fixed buffer zones, and the use of the Level 2 product reduces uncertainty related to emissivity over impervious and mixed urban surfaces.

E. Statistical Modeling

Land surface temperature at point level was modeled as a function of NDVI, NDMI, distance zone (0, 150, 300 m), year (1990, 2000, 2013, 2018), and their zone × year interaction [35], [36]. A linear mixed effects model with random intercepts for area and PointID (nested within area) was fitted [35]. The model was specified as follows (Eq. 3):

$$\begin{aligned}\mathrm{LST}_{ij} = \beta_0 &+ \beta_{NDVI} \cdot \mathrm{NDVI}_{ij} + \beta_{NDMI} \cdot \mathrm{NDMI}_{ij} \\ &+ \beta_{150} \cdot \mathrm{Z}_{150,ij} + \beta_{300} \cdot \mathrm{Z}_{300,ij} \\ &+ \beta_{2000} \cdot \mathrm{Y}_{2000,ij} + \beta_{2013} \cdot \mathrm{Y}_{2013,ij} \\ &+ \beta_{2018} \cdot \mathrm{Y}_{2018,ij} \\ &+ \beta_{150\times2000} \cdot \mathrm{Z}_{150,ij} \cdot \mathrm{Y}_{2000,ij} \\ &+ \beta_{150\times2013} \cdot \mathrm{Z}_{150,ij} \cdot \mathrm{Y}_{2013,ij} \\ &+ \beta_{150\times2018} \cdot \mathrm{Z}_{150,ij} \cdot \mathrm{Y}_{2018,ij} \\ &+ \beta_{300\times2000} \cdot \mathrm{Z}_{300,ij} \cdot \mathrm{Y}_{2000,ij} \\ &+ \beta_{300\times2013} \cdot \mathrm{Z}_{300,ij} \cdot \mathrm{Y}_{2013,ij} \\ &+ \beta_{300\times2018} \cdot \mathrm{Z}_{300,ij} \cdot \mathrm{Y}_{2018,ij} \\ &+ u_i + v_{j(i)} + \varepsilon_{ij}\end{aligned}$$

$$\begin{aligned}&u_i \sim N(0, \sigma^2_{Area}), \quad v_{j(i)} \sim N(0, \sigma^2_{PointID}), \\ &\varepsilon_{ij} \sim N(0, \sigma^2_{\varepsilon}), \quad u_i \perp v_{j(i)} \perp \varepsilon_{ij}\end{aligned} \quad (3)$$

$i = 1, \ldots, 4$; $j = 1, \ldots, N_i$ — PointID (30 m cell centroid) within site i

Note: "·" denotes multiplication; "×" appears only inside parameter labels for interactions.

Where:

LST_{ij}	land surface temperature at point j in area i [°C]
β_0	Intercept [°C]— expected LST for Zone = 0 m, Year = 1990 at

	NDVIz = NDMIz = 0 (after standardization)
$NDVI_{ij}$, $NDMI_{ij}$	standardized z-scores (grand-mean centered, unit variance) — continuous unitless covariates [43]
β_{NDVI}, β_{NDMI}	slopes [°C per 1 SD] — fixed effects
$Z_{150,ij}$, Z_{300}, ij	zone indicators (1 if 150 m/300 m; else 0); reference: 0 m.
$Y_{2000,ij}$, $Y_{2013,ij}$, $Y_{2018,ij}$	year indicators (1 if the given year; else 0); reference: 1990.
β_{150}, β_{300}	zone offsets vs. 0 m [°C] — fixed effects.
β_{2000}, β_{2013}, β_{2018}	year offsets vs. 1990 [°C] — fixed effects.
$\beta_{150\times2000}$, …, $\beta_{300\times2018}$	Zone×Year interaction effects [°C];
u_i	random intercept for Area *i*, $u_i \sim N(0, \sigma^2_{Area})$
$v_{j(i)}$	random intercept for PointID *j* within Area *i*, $v_{j(i)} \sim N(0, \sigma^2_{PointID})$.
ε_{ij}	residual error, $\varepsilon_{ij} \sim N(0, \sigma^2_{\varepsilon})$; mutually independent of the random effects[35]

Index i denotes the study site (i = 1…4). Index j denotes the PointID (30 m cell centroid) within site i. The model includes a random intercept for Area(i) to represent between site baseline differences, and a random intercept for PointID(j) within Area(i) to represent repeated measurements at the same 30 m location and time-persistent local conditions. Without these terms, correlation among the four yearly observations per location would lead to underestimated standard errors.

Marginal and conditional R^2 for the mixed model were obtained following Nakagawa and Schielzeth from the fitted specification. Denominator degrees of freedom for F-tests were computed with the Satterthwaite approximation, consistent with values reported in Tables III–IV and Supplementary Table S1.

NDVI and NDMI are included as continuous, pixel level covariates with global slopes estimated over the full set of sampled surfaces within the fixed buffers (vegetated and impervious). Thus, their coefficients represent population level averages rather than cover specific responses. This specification is adopted to retain parsimony alongside the Zone × Year structure and to avoid collinearity with categorical land cover factors. Cover specific stratification or interaction based terms are noted in the Discussion as beyond the present scope.

The LMM combines population-level fixed effects (β terms for NDVI, NDMI, zone, year, and their Zone × Year interactions) with random intercepts at the area and point levels (u_{Area} and $u_{PointID}$) to capture hierarchical data structure [35], [36]. Accounting for spatial clustering (points nested within areas) and repeated observations yields more precise coefficient estimates and supports valid inference on the effects of vegetation indices, zones, and years on LST [35], [36].

In this paper, park cool island is interpreted as a scene internal temperature contrast: the modeled mean LST in the park interior (0 m) compared with the modeled mean LST at 150 m and 300 m. These contrasts are obtained directly from the fixed Zone coefficients and the corresponding Zone×Year interactions (interior as the reference). To reflect heterogeneous surroundings without over parameterising the model, continuous NDVI and NDMI as pixel level covariates (fractional greenness and canopy moisture) were included rather than categorical land cover classes.

NDVI and NDMI were standardized to z-scores (mean 0, unit variance) prior to estimation to place the continuous predictors on a common scale, permitting direct comparison of their coefficients; for interpretability [43]. Hereafter, the standardized versions are denoted as NDVIz and NDMIz when needed (mean = 0, SD = 1). The effects were additionally reported per +0.10 and +0.05 index increments (a pure rescaling that does not alter point estimates, uncertainty, or inference). Model estimation was performed with lme4 [34]. The degrees of freedom of the denominator were obtained via the Satterthwaite approximation as implemented in lmerTest, and for fixed effects, Type-III F-tests were used [37]. Where informative, marginal and conditional R^2 are reported following [44], [45]. Residual structure was evaluated using residuals-versus-fitted and Q–Q plots. Collinearity was screened using variance-inflation factors (VIF) [46], and spatial autocorrelation of residuals was checked with Moran's I [47] within areas. Sum-to-zero contrasts (contr.sum) were used for categorical predictors so that Type-III tests are well-defined [37], [46]. Supplementary Material contains model-fit metrics (Table S1), 95% confidence intervals for fixed effects (Table S2), the full VIF table (Table S3), Moran's I with permutation p values (Table S4), and diagnostic plots (Figs. S1–S2). Modeled zone-by-year means are shown in Fig. 3. Observed LST distributions by zone and year are shown as boxplots in Fig. 4.

III. Results

A. Model Diagnostics

Model checks indicated that the assumptions of the linear mixed effects model were met. Residuals versus fitted values showed no heteroscedasticity or trend; points remained centered around zero across the range of fitted LST. The normal Q–Q plot exhibited only a slight S-shape, which is typical for very large samples (Supplementary Figs. S1–S2). Collinearity among fixed predictors was moderate to high (maximum VIF = 10.521; NDMIz = 7.205; NDVIz = 5.748; Supplementary Table S3), yet effects remained stable and precisely estimated [46]. Denominator degrees of freedom from the Satterthwaite approximation were large and 95% confidence intervals for fixed effects were narrow, indicating precise estimates.

For clarity, the coefficients of determination used later are defined here. The marginal coefficient R_m^2 denotes the share of variance explained by the fixed effects alone, whereas the conditional coefficient R_c^2 denotes the share explained by the full model (fixed + random effects); both were computed from the fitted LMM following Nakagawa and Schielzeth (Supplementary Table S1).

Residuals displayed positive local spatial autocorrelation within areas (k-nearest neighbours, k = 8): Moran's I ≈ 0.470 (Legowski), 0.438 (Planty), 0.465 (Wolski), and 0.323 (Zabierzowski), two-sided p = 0.01 for each (Supplementary Table S4). Because a complete 30 m grid is used within zones, such short-range dependence is expected and does not affect within-scene interior–buffer contrasts that underpin the inference (diagnostics in Figs. S1–S2; permutation tests in Table S4).

Evidence against overfit and singularity is as follows: no convergence warnings were issued; all random-effect variances were strictly positive (see Table II); residual-versus-fitted and Q–Q plots showed no systematic patterns; and the chosen mixed specification improved AIC relative to simpler linear alternatives (Supplementary Table S1).

B. Model Fit and Variance Components

The linear mixed effects model was fitted by restricted maximum likelihood (REML) [34]. Model selection references AIC (Akaike Information Criterion). The dataset comprised four areas, with 33,949 points nested within areas. The model achieved a high log-likelihood ($\approx -3.02\times10^5$) and AIC $\approx 6.04\times10^5$ (Supplementary Table S1). These values are expected given the large sample size. Nonetheless, comparisons to simpler linear models indicated substantially improved fit for the mixed model (lower AIC).

Model fit metrics (Supplementary Table S1) indicate that fixed effects explained 37.5% of LST variance ($R_m^2 = 0.375$), while including random intercepts increased the explained variance to 95.6% ($R_c^2 = 0.956$). This shows that park specific baselines account for a large share of variability beyond the global fixed effects.

The random effects intercept for Area accounts for a substantial share of unexplained variation ($\sigma_{Area}^2 \approx 11.611$, SD ≈ 3.408 °C) (Table II), reflecting persistent between-park differences in baseline LST. Additional heterogeneity is captured by the PointID term within areas ($\sigma_{PointID}^2 \approx 1.523$; SD ≈ 1.234 °C), while the residual variance was ≈ 1.002 (SD ≈ 1.001 °C), implying tight scatter around model predictions. Thus, after accounting for vegetation indices and the zone–year structure, most remaining variability is still attributable to differences between parks, with a smaller but non negligible contribution from location specific conditions.

All random-effect variances were strictly positive and the singular-fit check did not flag boundary estimates, consistent with an identifiable random-effects structure. Combined with the diagnostics in III-A and the AIC comparisons (Supplementary Table S1), this supports the statements that there were no signs of overfitting or singularity.

TABLE II

RANDOM-EFFECTS VARIANCES (AREA; POINTID WITHIN AREA)

Group	Variance	Std. Dev.
PointID:Area ($\sigma_{PointID}^2$)	1.523	1.234
Area (σ_{Area}^2)	11.611	3.408
Residual ($\sigma_{Residual}^2$)	1.002	1.001

Notes: Area = site-level random intercept; PointID:Area = random intercept for PointID nested in Area; Residual = within-point residual variance (see Supplementary Table S1 for values).

C. Fixed Effects of Vegetation, Zone, and Year

In Table III, NDMI, Zone, Year, and the Zone × Year interaction are all highly significant ($p < 0.001$). In contrast, NDVI is not significant once NDMI and the spatiotemporal terms are included ($F = 0.038$, $p = 0.846$). The dominant fixed effect is NDMI ($F = 15002.14$, $df = 1$, $p < 0.001$), followed by Year ($F = 31175.67$, $df = 3$, $p < 0.001$) and Zone ($F = 8795.19$, $df = 2$, $p < 0.001$). The significant Zone × Year term ($F = 269.25$, $df = 6$, $p < 0.001$) indicates that buffer contrasts vary across years.

These NDVI/NDMI coefficients should be interpreted as population level averages across the mixed surface types present in the buffers. While the overall inverse LST–index pattern holds at the dataset level, cover specific marginal effects may differ, for example NDVI saturation in dense vegetation or limited sensitivity over impervious pixels. Consistent with Table III, all terms except NDVI were statistically significant ($p < 0.001$). The estimates were precise, as indicated by narrow 95% confidence intervals (Table S2). After adjustment for the other terms (Table IV), higher canopy moisture (NDMI) was associated with cooler LST (β = −1.248 °C per 1 SD increase in NDMIz, SE = 0.010 °C; $p < 0.001$). Because NDMI was z standardized, this corresponds to −0.125 °C per 0.10 SD increase on the standardized scale.

Greenness (NDVI) does not provide an additional association with LST once NDMI and the other model terms are included (β = +0.002 °C per 1 SD increase in NDVIz, SE = 0.011 °C; $p = 0.846$). The contrast is particularly clear in 2000 for core zone samples: the NDMI–LST relation forms a steeper, more coherent band than the NDVI–LST relation (Fig. 2). The apparent horizontal streaks in Fig.2. reflect quantization due to the native thermal pixel size and the resampling to 30 m; several samples inherit the same thermal value from a single parent pixel. This is a plotting artefact and it does not affect inference, because the same sampled LST values are used consistently across predictors and years. Year by year bivariate plots for the core zone are provided in the Supplement (Figs. S3–S4), together with OLS statistics.

TABLE III

TYPE III ANOVA FOR FIXED EFFECTS.

Term	Sum Sq	NumDF	DenDF	F value	Pr(>F)
NDVI	0.038	1	135,778	0.038	0.846
NDMI	15,025	1	132,681	15002.14	<0.001
Zone	17,617	2	34,946	8795.19	<0.001
Year	93,669	3	112,038	31175.67	<0.001
Zone ×Year	1618	6	101,793	269.25	<0.001

Notes: Sum Sq = type-III sum of squares for the term; NumDF = numerator degrees of freedom; DenDF = denominator degrees of freedom (Satterthwaite approximation); F value = F-statistic for the term; Pr(>F) = p-value for the F-test.

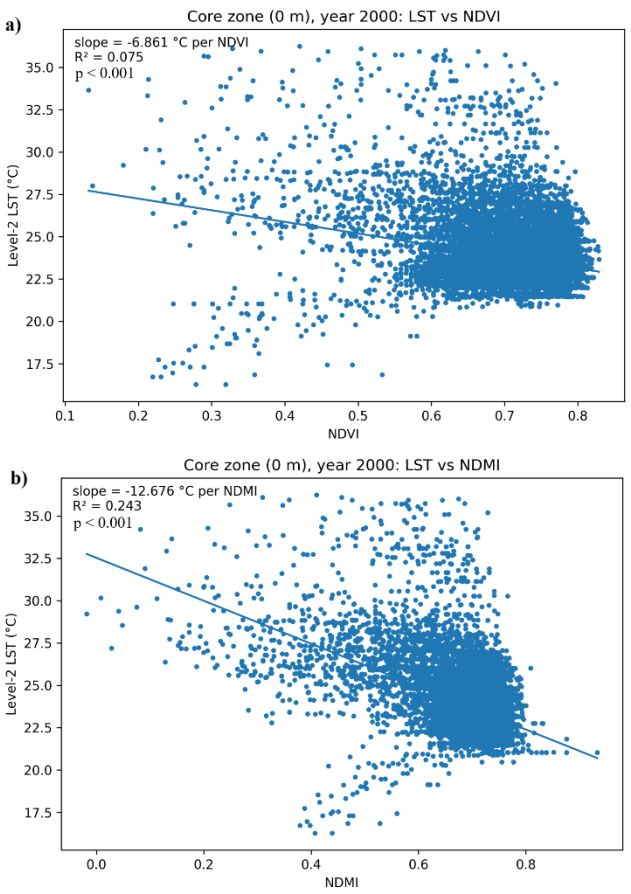

Fig. 2. LST versus vegetation indices for the core zone (0 m). (a) LST vs NDVI; (b) LST vs NDMI. Points represent 30 m samples from all sites; the solid line shows an ordinary least squares fit. The fitted slope, coefficient of determination (R^2), and the p value for the slope are reported in each panel. Both indices show negative associations with LST; in 2000 the NDMI slope and fit are significantly stronger than for NDVI (consistent with Table IV where standardized coefficients favor NDMI). Note: horizontal groupings of points occur because many 30 m samples share identical LST values inherited from the native thermal pixels (120 m for TM; 100 m for TIRS) after resampling the native thermal grid to 30 m with bilinear interpolation.

The model intercept of ~23.54 °C (SE = 1.704) corresponds to the expected LST in 1990 at a core zone location with average index conditions. These fixed effect (Table IV) estimates show that higher canopy moisture (NDMI), interior zones, and earlier years are associated with cooler surface temperatures.

The Zone (distance) main effect indicates a persistent park cool island gradient. Using the forest core (0 m zone) as baseline, the 150 m buffer zone is on average +2.140 °C warmer (SE = 0.021) and the 300 m zone is +2.632 °C warmer (SE = 0.022). These positive offsets are highly significant ($p < 0.001$) and imply that even in the baseline year, areas farther from the park interior experience elevated LST. Similarly, Year effects confirm an overall upward shift relative to 1990. Mean LST in the baseline zone increased by +3.757 °C in 2000, +3.606 °C in 2013, and +4.050 °C in 2018 (SE ≈ 0.01–0.03 °C for each). All year contrasts are significant ($p < 0.001$). The model intercept of ~23.54 °C (SE = 1.704) corresponds to the expected LST in 1990 at a core zone location with average NDVI/NDMI conditions. These fixed-effect (Table IV) estimates show that higher canopy moisture (NDMI), interior forest zones, and earlier years (1990) are associated with cooler surface temperatures. In contrast, lower NDMI, outer buffer zones, and later years correspond to higher LST. Type III tests with Satterthwaite denominator degrees of freedom show that all fixed terms except NDVI are statistically significant (Table III).

TABLE IV
FIXED EFFECTS FROM THE LINEAR MIXED EFFECTS MODEL

Term	Estimate (β, °C)	Std. Error (°C)	DenDF	t value
Intercept	23.541	1.704	3	13.82
NDVI	0.002	0.011	135,800	0.19
NDMI	-1.248	0.010	132,700	-122.48
Zone150	2.140	0.021	73,280	101.07
Zone300	2.632	0.022	74,280	118.21
Year2000	3.757	0.012	109,300	302.55
Year2013	3.606	0.028	132,800	129.88
Year2018	4.050	0.028	132,900	144.10
Zone150 × Year2000	0.503	0.018	100,600	27.70
Zone300 × Year2000	0.671	0.019	100,800	34.55
Zone150 × Year2013	0.089	0.019	104,000	4.73
Zone300 × Year2013	0.256	0.020	104,500	12.67
Zone150 × Year2018	0.198	0.019	104,300	10.46
Zone300 × Year2018	0.422	0.020	105,600	20.65

Note: Predictors NDVI, NDMI are standardized (SD=1), all terms are statistically significant at $p < 0.001$ except NDVI ($p = 0.846$), Zone and Year are indicator variables (baseline: interior zone, 1990).

D. Interaction Effects (Zone × Year)

The significant Zone × Year term indicates that the park cooling gradient (core vs. buffer temperature difference) varied across the years. In the model, the interaction coefficients are positive, meaning the outer zone LST was higher relative to the core than expected from main effects alone in certain years. The largest interaction effects occurred in Year 2000 (TABLE IV): an additional β = +0.503 °C in the 150 m zone and +0.671 °C in the 300 m zone (beyond their baseline offsets). Thus in 2000, the 150 m and 300 m zones were roughly 0.5–0.7 °C warmer relative to the core than in 1990, amplifying the core to edge temperature contrast. By Year 2013, the interaction terms were smaller (+0.089 °C and +0.256 °C for 150 m and 300 m). This indicates a reduced additional widening of the thermal gradient compared with 2000, particularly for 150 m. In Year 2018, the interactions increased again to +0.198 °C (150 m) and +0.422 °C (300 m), indicating a moderate re-widening of the thermal gradient by the end of the period. All these interaction estimates are statistically significant ($p < 0.001$), owing to the large sample size, but their magnitudes are what convey practical relevance. The pattern can be summarized as follows: the forest interior was consistently coolest in all years, but the core to periphery LST contrast peaked around 2000, then diminished by 2013, and increased again by 2018. This temporal modulation of the park cool island intensity is evidenced by the

Zone × Year profile (Table IV). This interaction profile is visible as the varying separation of the zone specific lines across years in Fig. 3.

E. LST Patterns by Zone and Year

The modeled mean LST for each zone and year is shown in Fig. 3. Because zone contrasts are computed within the same clear sky scene, they are insensitive to any scene wide LST bias and can be read as robust zone differences rather than absolute temperatures. Across the parks, the pattern is consistent. Planty contributes only to the 0 m and 150 m zones, and the 300 m contrasts are based on the three sites with a defined 300 m ring. For the 150 m buffer, the model implied an average offset relative to the core of +2.140 °C in 1990, +2.643 °C in 2000, +2.230 °C in 2013, and +2.338 °C in 2018. For 300 m, the corresponding offsets are +2.632 °C (1990), +3.303 °C (2000), +2.888 °C (2013), and +3.055 °C (2018). Thus, the 0 m to 300 m contrast was largest in 2000, smaller in 2013, and intermediate in 2018, consistent with the significant Zone × Year interaction. When combining the intercept and year effects, the expected interior LST is about 23.54 °C in 1990, 27.30 °C in 2000, 27.15 °C in 2013, and 27.59 °C in 2018, at average NDVI/NDMI conditions.

Two features are evident: (i) a persistent interior-to-edge gradient and (ii) an upward shift of all zones over time. The 0 m line lies lowest in every year (Fig. 3), while the 150 m and 300 m lines are higher by amounts implied by the zone and interaction terms. Year effects shift all zone means upward across the period. Fig. 3a shows that observed zone-by-year means track the model-based profiles closely; the two sets of lines lie near each other across all years and zones. Fig. 3b visualizes the interior versus buffer separation for 0 m, 150 m, and 300 m in each year; the magnitude of the separation varies with time, in line with the significant Zone × Year term reported in Tables III–IV. The dashed observed trajectories closely track the solid model-based means in each zone, while the separation among 0 m, 150 m, and 300 m lines visualizes the distance decay of PCI across years; the corresponding observed distributions are shown as boxplots in Fig. 4.

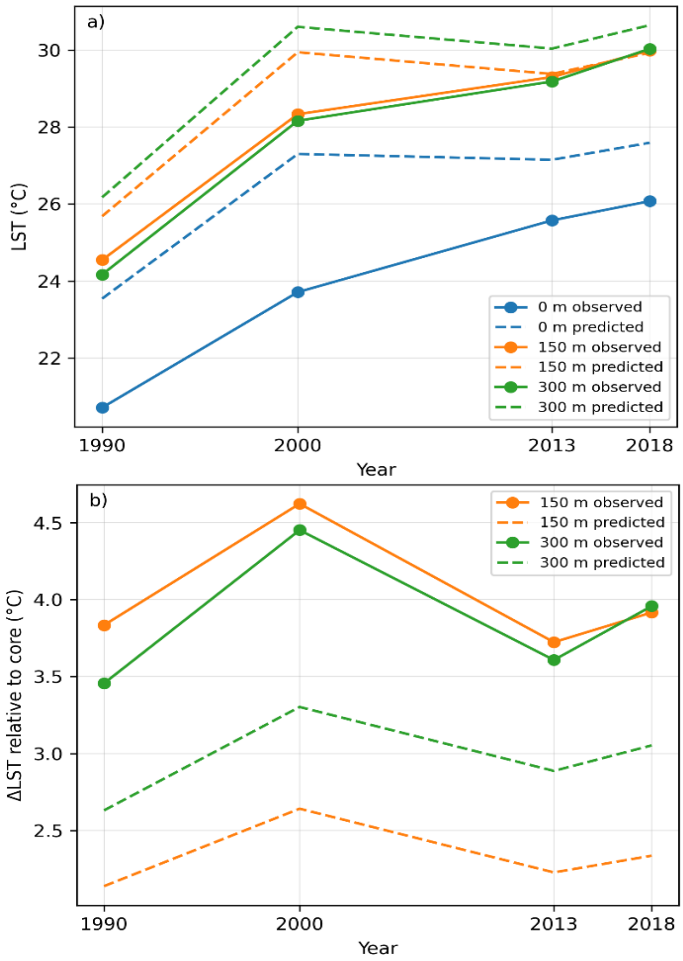

Fig. 3. Observed and model based LST by zone and year. a) Observed (dashed) and predicted (solid) zone by year mean LST for 0 m interior, 150 m, and 300 m. Predicted values come from the fixed part of the mixed model at NDVIz=NDMIz=0 (Eq. 3); b) Zone profiles (0 m, 150 m, 300 m) across years (1990, 2000, 2013, 2018) illustrating the interior versus buffer gradient and its temporal change consistent with the Zone × Year effects. Note: Planty contributes only to the 0 m and 150 m zones; the 300 m means are based on the remaining sites.

Observed LST distributions by zone and year (Fig. 4) show interiors cooler than buffers in all parks and all years, consistent with the modeled means. The increase from interior to outer buffer is stronger in Wolski and Zabierzowski than in Planty (0–150 m only), which is a compact downtown park; Legowski Forest (about 24 ha) shows an intermediate pattern that reflects a small riparian footprint and strong edge influence. These site-wise differences align with canopy continuity and surrounding urban fabric and are consistent with the random Area variance reported earlier.

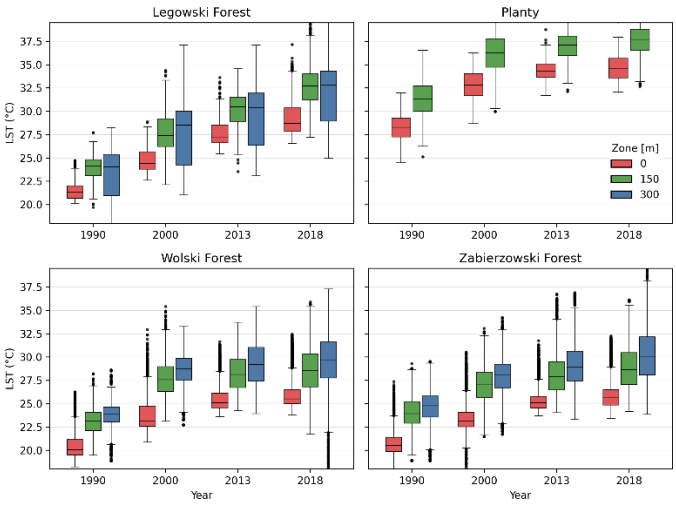

Fig. 4. Observed LST distributions by zone and year for each park (boxplots for interior 0 m, 150 m, and 300 m where available; years 1990, 2000, 2013, 2018). For Planty, the 150–300 m ring contains no pixels mapped as vegetation and is therefore not shown or used in the mixed model.

TABLE V
PARK SIZE AND OBSERVED LST CONTRASTS BETWEEN INTERIOR AND BUFFER ZONES (FOUR EPOCHS)

Park	**Area (ha)**	**Morphology and setting**	**ΔT150 mean (range), °C**	**ΔT300 mean (range), °C**	**Cooling extent evidence in zone summaries**
Wolski Forest	419	Large, contiguous forest park on the urban fringe	2.32 (1.98–2.97)	2.65 (2.22–3.36)	Core to buffer contrast present at 150 m and 300 m
Zabierzowski Forest	387	Large forest area with continuous canopy cover	2.22 (1.90–2.54)	2.51 (2.18–2.86)	Core to buffer contrast present at 150 m and 300 m
Legowski Forest	24	Small riparian forest patch, high edge exposure	2.19 (1.75–2.88)	2.54 (1.94–3.22)	Core to buffer contrast present at 150 m and 300 m, with larger interannual variation
Planty	21	Narrow ring shape urban park in the dense historic core	2.09 (1.89–2.29)	n/a	300 m zone not defined for Planty

To make the cross park differences more explicit, Table V summarises park size and observed LST contrasts between the interior and the surrounding buffers for each epoch. Here, ΔT150 and ΔT300 are defined as the buffer mean LST minus the core mean LST, so positive values indicate warmer surroundings. The two large forest parks (Wolski, 419 ha; Zabierzowski, 387 ha) show an interior to buffer contrast that remains evident at both 150 m and 300 m from the boundary. Across the four scenes, the mean ΔT at 300 m equals 2.65 °C for Wolski (range 2.22–3.36 °C) and 2.51 °C for Zabierzowski (range 2.18–2.86 °C). This indicates that, in these contiguous forest sites, the interior advantage extends beyond the immediate edge. The smaller riparian forest (Legowski, 24 ha) shows comparable contrasts on average (mean ΔT300 2.54 °C, range 1.94–3.22 °C), but with larger interannual variability, consistent with stronger edge exposure and a more heterogeneous buffer environment. Planty (about 21 ha) is embedded in the dense historic core and forms a narrow ring shaped green space; an interior to 150 m contrast remains evident (mean ΔT150 2.09 °C, range 1.89–2.29 °C). The 300 m zone is not defined for Planty because the 150 to 300 m band contains no UA2018 vegetation pixels in this city center context (Fig. 4). With four parks, this comparison is descriptive, but it makes the role of park size and geometry transparent in the observed contrasts.

The magnitude of the zone contrast varies by year in line with the significant Zone × Year interactions (Table IV). Relative to the 0 m baseline, the 150 m offsets equal 2.140 °C in 1990 and 2.643 °C in 2000, then 2.229 °C in 2013 and 2.337 °C in 2018 (zone main effect plus interaction). For 300 m the corresponding offsets are 2.632 °C (1990), 3.303 °C (2000), 2.888 °C (2013), and 3.053 °C (2018). Thus, the interior to edge gradient is steepest around 2000, smallest in 2013, and intermediate in 2018 (Table IV).

At the mean of the standardized indices ($z = 0$), expected interior LST is ~23.54 °C in 1990; adding the year coefficients gives ~27.30 °C (2000), ~27.15 °C (2013), and ~27.59 °C (2018). The year terms indicate an overall upward shift relative to 1990, whereas the persistent separation of the zone lines shows that the interior advantage remains in each epoch.

IV. DISCUSSION

A. Key Quantitative Findings and NDMI vs. NDVI Performance

The four sites differ in area, canopy continuity, and surrounding urban fabric, and these differences are visible in both the modeled contrasts and the observed distributions. The random Area effect ($\sigma^2 \approx 11.611$; SD ≈ 3.41 °C) quantifies substantial baseline differences among parks, with Wolski is consistently coolest and Planty is warmest, with Zabierzowski and Legowski in between. The interior-to-buffer rise is stronger in the two large forest sites than in the compact downtown park, which aligns with greater canopy continuity and a less impervious context. Site-wise Moran's I of residuals supports these contextual differences (Table S4). At the same time, the long-term analysis indicates a clear upward shift in daytime LST across the four late-spring scenes: relative to 1990, the year effects imply an increase of about 4.05 °C by 2018 (Table IV) [4], [8]. Despite this background warming, parks retained a robust daytime cool island signal. Model based core to buffer contrasts were ~2.14–2.64 °C for the 150 m buffer and ~2.63–3.30 °C for the 300 m buffer across years (Table IV, Fig. 3), indicating a consistent distance decay pattern and persistent cooling relative to the surroundings [10], [11]. Across the four

parks, both the observed distributions and the mixed effects model show a persistent interior to buffer temperature gradient. Model based offsets indicate that the 150 m ring was warmer than the core by 2.140 °C in 1990, 2.643 °C in 2000, 2.230 °C in 2013, and 2.338 °C in 2018. For the 300 m ring, the corresponding differences are 2.632 °C, 3.303 °C, 2.888 °C, and 3.055 °C (Table IV; Fig. 3). In parallel, Table V indicates that the observed mean contrasts are of comparable magnitude, with mean interior to 150 m differences around 2.1–2.3 °C across parks and years, and mean interior to 300 m differences around 2.5–2.7 °C in the three parks where a vegetation masked 300 m ring is available. Under comparable late morning clear sky conditions, expected interior LST increased relative to 1990 by about 3.6–4.1 °C across the later scenes (Table IV), yet the interior cooling advantage remained evident in every epoch. These magnitudes are consistent with reported daytime surface PCI ranges for mid latitude urban parks[10], [11], [13], [27]. Vegetation moisture was the dominant vegetation predictor of LST in this dataset. After standardization, NDMI is associated with a −1.248 °C change in LST per one standard deviation ($p < 0.001$), whereas NDVI shows no additional association once NDMI and the spatial and temporal terms are included ($p = 0.846$) (Tables III–IV). NDVI remains a useful proxy of canopy amount [16], but it does not represent water status and can saturate in dense canopies. NDMI and related water indices respond to vegetation liquid water content [39] and therefore better reflect conditions that support evaporative cooling. NDVI and NDMI are correlated (NDMI VIF about 7; Table S3), but the NDMI association remains strong in the joint model. From a management perspective, the result points to water availability as a practical lever for surface cooling, alongside canopy cover, particularly during warm periods [30]. Taken together, the pattern is consistent with urban heat island dynamics being modulated by vegetation and water availability [5].

B. Comparison with Other Studies

The cooling magnitude estimated for the analyzed areas is consistent with reports from other cities. Reviews indicate that urban green areas are on average about 1 °C cooler than nearby built up terrain, with larger differences in specific settings [10], [11]. Daytime park cool island intensities of about 1–5 °C have been documented in different climates and study designs [12], [13], [16]. In the analyzed dataset, the observed mean interior to buffer contrasts are larger than 1–2 °C. Table V indicates mean interior to 150 m differences around 2.1–2.3 °C across parks and years, and mean interior to 300 m differences around 2.5–2.7 °C in the three parks where a vegetation masked 300 m ring is available. Consistently, the model based offsets range from 2.140 to 2.643 °C at 150 m and from 2.632 to 3.303 °C at 300 m, depending on year (Table IV; Fig. 3). These values remain within the broader range of daytime surface PCI magnitudes reported for urban parks across climates and study designs[12], [13], [16], and the spatial reach is consistent with observations that cooling can extend a few hundred meters beyond park boundaries[16], [28].

Differences in vegetation help explain the strength of the effect. Areas with many trees usually cool more than small parks or lawns, because tree canopies sustain higher transpiration and increase aerodynamic roughness, which supports convective heat loss [17], [19], [22]. Results across Europe likewise show that districts with substantial tree cover are about 8–12 °C cooler in summer land surface temperature than dense built up districts, whereas treeless green spaces are cooler by only about 2–4 °C [20].

Open water can strengthen park cooling through evaporation [10], [21]. As no large water bodies are present in the analyzed areas, the reported values reflect primarily vegetation effects. Even without lakes or ponds, the magnitude of cooling and its decay with distance are in line with established park cool island behavior [11], [12].

C. Park Cool Island Persistence and Mechanisms

A key question was whether the parks' cooling effect could withstand long-term warming. The PCI in Krakow remained remarkably stable over nearly three decades. The interior–edge temperature difference did not diminish despite ~5 °C of regional summer warming and ongoing urbanization. This means that in 2018, there was a comparable decrease in LST relative to the surrounding area as in 1990. This persistence underscores the resilience of well-vegetated parks as urban climate moderators. It also aligns with observations from other regions. Global satellite analyses report that forested parks maintain robust cooling even under heatwaves or droughts. In contrast, sparsely vegetated open spaces suffer greater performance losses in extreme conditions [23], [27]. Across the four epochs, cooler park interiors relative to the surrounding buffers were consistently observed, while the magnitude of the contrast varied in time. The larger interior to buffer contrast in 2000 and its reduction by 2013 indicate temporal modulation rather than a monotonic trend. Several factors can contribute to this pattern, including interannual differences in atmospheric moisture and antecedent conditions at the time of image acquisition, as well as gradual land cover change within the fixed buffer zones. Because only four clear sky late spring scenes were analyzed and time resolved land cover change information was not incorporated, these drivers cannot be separated here. Interpretation therefore focuses on the observed within scene thermal contrasts, while acknowledging that part of the long term modulation may reflect changes in the surroundings rather than changes in park functioning. The lower daytime temperatures observed in this study, approximately 1.5°C lower in the depths of parks, are comparable to the average intensity of surface PCI worldwide (~1–2°C) [10], [11]. Despite nearly 30 years of urban growth and rising regional temperatures, the inner zones of these parks did not experience as extreme an LST increase as their surroundings – effectively preserving a local "cool island" microclimate. Similar longitudinal evidence of stable or even growing park cool islands has been reported in other contexts. The results obtained for Krakow's forests confirm that protecting and strengthening urban green infrastructure can continuously offset part of urban background warming. A plausible explanation is that the expansion of the city's built-up area and heat output over the years was counterbalanced by the parks' unchanged or even improved vegetation characteristics (mature tree growth, etc.). Thus, the parks provided a roughly steady cooling service. The results showed that urban parks can reliably mitigate excess heat locally, even as broader climate

warming occurs. This underscores their value as a long term climate-adaptation measure.

D. Limitations and Future Research

Several limitations should be acknowledged. Land surface temperature was taken from the Landsat Collection 2 Level 2 surface temperature product, which applies atmospheric correction and emissivity processing and provides per pixel quality flags [41], [42]. This reduces sensitivity to emissivity uncertainty over impervious and mixed urban surfaces compared with simplified thermal retrieval workflows, but residual uncertainty can remain near edges and in heterogeneous buffers due to mixed thermal pixels and sub pixel land cover composition. For this reason, the interpretation emphasizes within scene contrasts between the park interior and the fixed buffer zones rather than absolute LST values.

A second limitation concerns temporal sampling. The analysis relies on four Landsat acquisitions (1990, 2000, 2013, 2018), each representing a single clear sky May scene selected to control phenology and to minimize cloud contamination. This design supports a controlled comparison across epochs, but it does not provide a temporally continuous record and it does not capture seasonal heterogeneity. As a result, the reported differences should be read as multi epoch snapshots rather than a continuous long term trajectory, and cooling dynamics outside late spring remain unresolved.

Furthermore, the magnitude of the PCI temperature contrast naturally reflects the land cover mosaic immediately outside park boundaries (impervious vs. vegetated context). In this modeling this context is partly captured through continuous NDVI/NDMI at the pixel level; an explicit land cover stratification was intentionally not included to retain parsimony in this multi decadal, phenology controlled analysis and is noted as a limitation. The model focuses on relative, within scene contrasts under clear sky May conditions; while this reduces short term weather noise, it does not represent all sky conditions and may under or over state contrasts relative to other seasons. Therefore PCI was interpreted as a robust relative temperature difference rather than an absolute cooling flux.

Satellite-derived LST represents the land surface "skin" temperature under clear sky daytime conditions. This can differ from ambient air temperature at 2 m height. Night-time or cloudy conditions were not captured. Because the largest UHI and PCI contrasts are typically produced under clear, sunny conditions [48], the reported cooling magnitudes likely represent an upper bound under typical conditions. Actual benefits to human thermal comfort depend on air temperature moderation, shade (which directly affects perceived temperature). In addition, humidity/wind factors. Field measurements with meteorological sensors in and around the parks would complement the findings by quantifying air cooling and human comfort indices. Some studies have measured urban park air temperature differences on the order of ~1–5 °C (parks cooler) depending on park size and time of day [11], [12], [13]. However, more localized monitoring in Krakow would reveal how the ~2–3 °C surface cooling translates into perceived cooling for residents. Second, the 30 m spatial resolution of Landsat smooths over sharp micro-scale gradients. Fine features like narrow park edges, small water bodies, or isolated trees are not fully resolved, potentially underestimating peak cooling right at the boundary or over small ponds [15]. Mixed land-cover within pixels (e.g. a single 30 m cell containing both vegetation and pavement) could also dilute measured temperature differences. Higher-resolution thermal imagery (e.g. 1–5 m from drones, or ~70 m from ECOSTRESS) and geostatistical downscaling could help capture these fine-scale effects. The Landsat overpass (~11:30 AM local) means that surface temperatures were analyzed in the late morning – a useful period when heating is underway. However, not necessarily the day's peak. It is possible that in the middle of the afternoon the intensity of cool islands in parks varies, or that after sunset the cooling contrast changes. Maximum air temperature contrast can occur later in the day and in the evening under calm conditions, when parks cool faster than surrounding built surfaces [49]. Night-time cooling islands in parks have not been studied. Under clear, calm nights parks sometimes cool faster than urban surroundings, creating a strong air temperature cool island, although in certain cases complex effects like cold-air drainage can reverse this (the so-called "park heat island") in specific terrain [27].

Third, the use of NDVI and NDMI indices as explanatory variables, although informative, has caveats. These spectral indices are approximate values of vegetation amount and moisture. They do not capture all aspects of land cover. NDVI can saturate in very dense vegetation (losing sensitivity to additional biomass) and is insensitive to differences among vegetation types (e.g., grass, shrubs, and trees can produce similar NDVI values). NDMI is sensitive to canopy water status, but it can also be affected by background reflectance in sparse canopies and by mixed pixels in urban settings [39]. Thus, these indices are imperfect representations of the complex biophysical processes governing cooling. Including variables like leaf area index (LAI), canopy height, or 3D structure (from LiDAR) could improve future models. The properties of the built environment (e.g. building height, street canyon geometry) in the vicinity were also not explicitly taken into account. This might influence how far park cooling extends. These factors have been partially taken into account in the random effects specific to a given area and in the categorization of buffer zones. However, a more detailed treatment (e.g. local sky view factor or impervious fraction around each point) would be a useful extension [40]. These limitations motivate the integration of structural and flux metrics to clarify the mechanisms linking spectral moisture to surface cooling. To strengthen the mechanistic interpretation of the NDMI–LST relationship, advanced remote sensing and ecological modeling can be integrated. Canopy structure can be characterized with LiDAR to obtain canopy height, crown depth, and gap fraction; these attributes influence aerodynamic roughness, shading, and transpiration efficiency. Productivity can be represented by gross primary production estimated with process model guided transfer learning that fuses remote sensing features with ecophysiological constraints [50] Complementary water and energy flux metrics, including evapotranspiration, could also help interpret moisture related cooling, using remote sensing driven energy balance or hydrological modelling constrained by meteorological forcing. Within the mixed effects framework, such variables can be included as additional fixed effects or mediators to test whether

the moisture signal captured by NDMI operates through enhanced latent heat flux and sustained carbon uptake. Land cover change within the fixed buffer zones is a source of uncertainty. Buffer zones were delineated from a 2018 land cover dataset and applied consistently to earlier years. The built up fraction and land use within these buffers may have changed between 1990 and 2018, independent of any park driven cooling. For example, infill development or new impervious surfaces near park boundaries would increase buffer LST and enlarge the apparent contrast, even if the park itself remained stable. Conversely, urban greening or reduced imperviousness in the buffer could reduce the contrast. Because LST was taken from the Landsat Collection 2 Level 2 surface temperature product, atmospheric and emissivity processing is handled in a consistent operational framework [41], [42]. Still, land cover transitions within a fixed buffer can alter the physical drivers of LST and should be treated as an additional source of uncertainty in interpreting multi decadal PCI change [51]. NDVI and NDMI describe vegetation amount and moisture at the pixel level in each epoch and therefore capture part of the evolving surface state, but they do not provide an explicit measure of imperviousness or a complete accounting of land cover transitions. For this reason, the reported long term PCI modulation should be interpreted as a combined outcome of park conditions and contemporaneous change in the surrounding urban fabric. Future work could reduce this uncertainty by incorporating time series of impervious surface fraction or other land cover change indicators for each epoch, using products that are consistent with the Landsat record [40], [51].

Future work can also address the sparse temporal sampling by reconstructing denser time series from incomplete satellite observations. Recent methods provide practical approaches for gap filled vegetation index time series reconstruction and for densifying Landsat time series through combined filling and fusion strategies, including implementations in cloud platforms. These approaches could support seasonally resolved analyses and more continuous assessment of PCI variability. The references suggested by the reviewer are included as examples of such methods [52], [53], [54].

E. Practical Implications for Urban Heat Mitigation

The clear importance of vegetation moisture for cooling has direct implications for urban climate adaptation. This is consistent with the mixed model results, where NDMI shows a strong independent association with lower LST, while NDVI does not add explanatory power once moisture and the zone and year terms are included (Tables III–IV). Any irrigation-based interventions should be paired with water-sensitive design (e.g., reclaimed water, rainwater harvesting) to balance cooling benefits against water availability and sustainability constraints [30]. The results suggest that keeping urban green spaces well-hydrated can significantly enhance their cooling performance. Simply having trees or lawns is not enough – those plants must also have access to sufficient water to maximize transpiration. Urban planners and park managers should therefore consider measures to maintain high soil and vegetation moisture levels in and around parks. For example, strategic irrigation during heat waves or extended dry periods can boost cooling. Empirical observations indicate that well-watered vegetation can substantially outperform water-stressed vegetation in cooling efficacy [23]. On a city-wide scale, modeling studies suggest that systematically irrigating urban green spaces could reduce urban air temperatures by roughly 1–2 °C on average, with the largest benefits (up to ~1.5–2 °C cooling) in hot, dry climates [30]. Implementing irrigation infrastructure (using reclaimed water or harvested rainwater to supply parks during droughts) could thus be a viable heat mitigation strategy, especially under future warming. Of course, this must be balanced against water availability and sustainability concerns. However, technologies like smart drip irrigation and soil moisture sensors can optimize water use for cooling benefit. Additionally, tree species selection and landscape design should prioritize plant communities that both transpire at high rates and tolerate periodic drought. Some tree species have traits that allow them to continue transpiring and providing cooling even in hot, dry weather. In contrast, others shut down or drop leaves under heat stress [23]. Selecting drought-tolerant species with high transpiration rate (or mixes of species to ensure resilience) can make park cooling more reliable during extreme heat events. Urban forestry programs might focus on species known to sustain transpiration and recover quickly after water stress [23], combined with practices like mulching and soil improvement to enhance water retention. In practice, the findings imply that during extreme heat events, watering large parks and urban forests could measurably reduce surface temperatures, creating cooler refuge areas for the public.

Another practical consideration is the land-use planning around park edges. A persistent temperature gradient between the interior and the periphery has been observed, which means that the benefits of a cool park may be partially offset by the heat coming from its immediate surroundings. This suggests that maintaining buffer zones of lower-intensity development or additional greenery around major parks would help extend the cooling effect. If a park is immediately ringed by tall buildings, wide roads, or other heat-generating surfaces, the cool island may dissipate more abruptly at the boundary. Conversely, creating transitional green belts – such as tree-lined streets, community gardens, or small “stepping-stone” parks within the first 100–300 m of a large park – can expand and sustain the cooling influence into the neighborhood [9]. City planners should incorporate such green buffers in zoning and development plans to preserve a park’s cooling footprint. Limiting new construction or impervious surfaces right at the park perimeter, and promoting the creation of green infrastructure in that zone, are additional approaches to protect and magnify the park’s microclimate benefits for local residents. Linking small parks and street trees to form “cooling corridors” can create a more continuous cool island effect at the district scale [9]. The buffer analysis conducted in Krakow showed significant cooling up to 300 m, and other studies have noted park influences extending even several hundred meters further under favorable conditions (e.g. at night or with prevailing winds). Therefore, urban design should treat large parks as anchors of a broader cooling network, with deliberate greening of the surrounding areas to propagate the cool island.

Finally, from a broader perspective, a scalable method for quantifying park cooling effects is demonstrated, which can be replicated in other cities. By using standardized open datasets (multi-temporal Landsat thermal imagery and pan-European land-cover maps) and a consistent analytical framework, different cities can assess their own park cool islands in a comparable way. Such cross-city analyses would enable policymakers to benchmark how much cooling their urban forests provide relative to others [27]. This information can guide regional climate resilience efforts – for example, by setting evidence-based targets for urban green space conservation or restoration. The findings reinforce that investing in urban forests and well-watered greenery is a viable heat mitigation strategy in the face of climate change. Protect and expand large vegetated areas, and ensure adequate water supply (via irrigation or water-sensitive design). In addition, preserving some undeveloped buffer around them can collectively magnify their cooling impact on the city [23]. These actions will help enhance urban resilience to heat by leveraging nature-based solutions. Forested parks – especially those rich in trees and moisture – act as valuable long-term cooling assets for cities. Thoughtful planning and management can maximize their thermal benefits for urban populations now and in the future.

V. Conclusion

Multi-temporal Landsat thermal data were combined with a mixed effects framework to quantify how vegetation greenness (NDVI), canopy moisture (NDMI), distance from park cores, and year relate to urban LST in Krakow. Forest interiors remained significantly cooler than their surroundings, with park cool island effects on the order of ~2–3 °C (depending on buffer distance) under clear sky late spring conditions. This cooling gradient persisted over nearly three decades even as absolute temperatures rose by about 4 °C in the region, highlighting the enduring value of urban green spaces in a warming climate. Notably, the vegetation moisture index (NDMI) was a far stronger predictor of lower LST than the traditional greenness index (NDVI), suggesting that well-watered, moisture-rich canopies yield the greatest cooling benefits. Urban heat mitigation depends not only on green-cover extent but also on vegetation water status. From a planning perspective, the findings support the protection and expansion of forest areas in cities and the implementation of measures (such as irrigation or water-conscious urban design) to maintain high canopy moisture levels during hot periods. The use of standard Copernicus Urban Atlas boundaries and Landsat Collection-2 data in this study allows this analysis to be replicated in other cities, providing a basis for regional comparisons of park-cooling effectiveness. Forested parks act as long term cooling assets for cities, and strategies that enhance vegetation moisture and preserve buffer zones can magnify their cooling impact, contributing to urban climate resilience in the face of global warming. A key finding is that vegetation moisture (NDMI) is a stronger and more consistent predictor of lower LST than greenness (NDVI), underscoring the need to account for plant water status in urban-heat mitigation. In addition, this study adds multi-decadal evidence from a Central European city that forested parks maintain a persistent daytime cooling advantage despite regional warming.

Conflict of Interest – The authors declare no conflict of interest.

Data Availability — Landsat Collection-2 L2 products used in this study are available from USGS (product IDs listed in Table I). Derived datasets and R scripts for LMM and figure generation will be shared upon reasonable request.

References

[1] I. D. Stewart and T. R. Oke, “Local climate zones for urban temperature studies,” *Bull Am Meteorol Soc*, vol. 93, no. 12, pp. 1879–1900, 2012.

[2] M. Santamouris, “Urban heat island: Mechanisms, implications, and possible remedies,” *Annu Rev Environ Resour*, vol. 40, pp. 261–298, 2015, doi: 10.1146/annurev-environ-102014-021155.

[3] J. A. Voogt and T. R. Oke, “Thermal remote sensing of urban climates,” *Remote Sens Environ*, vol. 86, no. 3, pp. 370–384, 2003.

[4] N. Clinton and P. Gong, “MODIS detected surface urban heat islands and sinks: global locations and controls,” *Remote Sens Environ*, vol. 134, pp. 294–304, 2013.

[5] D. Zhou *et al.*, “Satellite remote sensing of surface urban heat islands: progress, challenges, and perspectives,” *Remote Sens (Basel)*, vol. 11, no. 1, p. 48, 2019, doi: 10.3390/rs11010048.

[6] Q. Weng, “Thermal infrared remote sensing for urban climate and environmental studies: methods, applications, and trends,” *ISPRS Journal of Photogrammetry and Remote Sensing*, vol. 64, no. 4, pp. 335–344, 2009, doi: 10.1016/j.isprsjprs.2009.03.007.

[7] M. L. Imhoff, P. Zhang, R. E. Wolfe, and L. Bounoua, “Remote sensing of the urban heat island effect across biomes in the continental USA,” *Remote Sens Environ*, vol. 114, no. 3, pp. 504–513, 2010, doi: 10.1016/j.rse.2009.09.012.

[8] S. Peng *et al.*, “Surface urban heat island across 419 global big cities,” *Environ Sci Technol*, vol. 46, no. 2, pp. 696–703, 2012, doi: 10.1021/es2030438.

[9] S. E. Gill, J. F. Handley, A. R. Ennos, and S. Pauleit, “Adapting cities for climate change: the role of the green infrastructure,” *Built Environ*, vol. 33, no. 1, pp. 115–133, 2007, doi: 10.2148/benv.33.1.115.

[10] K. R. Gunawardena, M. J. Wells, and T. Kershaw, “Utilising green and blue space to mitigate urban heat island intensity,” *Science of The Total Environment*, vol. 584–585, pp. 1040–1055, 2017, doi: 10.1016/j.scitotenv.2017.03.156.

[11] D. E. Bowler, L. M. Buyung-Ali, T. M. Knight, and A. S. Pullin, “Urban greening to cool towns and cities: a systematic review of the empirical evidence,” *Landsc Urban Plan*, vol. 97, no. 3, pp. 147–155, 2010, doi: 10.1016/j.landurbplan.2010.05.006.

[12] R. A. Spronken-Smith and T. R. Oke, "The thermal regime of urban parks in two cities with different summer climates," *Int J Remote Sens*, vol. 19, no. 11, pp. 2085–2104, 1998, doi: 10.1080/014311698215784.

[13] F. Aram, E. Higueras García, E. Solgi, and S. Mansournia, "Urban green space cooling effect in cities," *Heliyon*, vol. 5, no. 4, p. e01339, 2019, doi: 10.1016/j.heliyon.2019.e01339.

[14] Q. Xie and J. Li, "Detecting the cool island effect of urban parks in Wuhan: a city on rivers," *Int J Environ Res Public Health*, vol. 18, p. 10132, 2021, doi: 10.3390/ijerph182010132.

[15] G. L. Feyisa, K. Dons, and H. Meilby, "Efficiency of parks in mitigating urban heat island effect: an example from Addis Ababa," *Landsc Urban Plan*, vol. 123, pp. 87–95, 2014, doi: 10.1016/j.landurbplan.2013.11.014.

[16] X. Chen, Y. Zhang, X. He, C. Zhang, and J. Huang, "How to quantify the cooling effect of urban parks? Linking maximum and accumulated indicators," *Remote Sens Environ*, vol. 237, p. 111548, 2020, doi: 10.1016/j.rse.2019.111548.

[17] C. D. Ziter, E. J. Pedersen, C. J. Kucharik, and M. G. Turner, "Scale-dependent interactions between tree canopy cover and impervious surfaces reduce daytime urban heat during summer," *Proceedings of the National Academy of Sciences*, vol. 116, no. 15, pp. 7575–7580, 2019, doi: 10.1073/pnas.1817561116.

[18] L. Shashua-Bar and M. E. Hoffman, "Vegetation as a climatic component in the design of an urban street," *Energy Build*, vol. 31, no. 3, pp. 221–235, 2000.

[19] D. Armson, P. Stringer, and A. R. Ennos, "The effect of tree shade and grass on surface and globe temperatures in an urban area," *Urban For Urban Green*, vol. 11, no. 3, pp. 245–255, 2012, doi: 10.1016/j.ufug.2012.05.002.

[20] J. Schwaab, R. Meier, G. Mussetti, S. I. Seneviratne, C. Bürgi, and E. L. Davin, "The role of urban trees in reducing land surface temperatures in European cities," *Nat Commun*, vol. 12, p. 6763, 2021, doi: 10.1038/s41467-021-26768-w.

[21] R. Sun and L. Chen, "How can urban water bodies be designed for climate adaptation?," *Landsc Urban Plan*, vol. 105, no. 1–2, pp. 27–33, 2012.

[22] S. C. Zipper, J. Schatz, C. J. Kucharik, and S. P. I. I. Loheide, "Urban heat island–induced increases in evapotranspirative demand," *Environmental Research Letters*, vol. 12, no. 9, p. 094008, 2017, doi: 10.1088/1748-9326/aa8f8b.

[23] H. Li, Y. Zhao, C. Wang, D. Ürge-Vorsatz, J. Carmeliet, and R. Bardhan, "Cooling efficacy of trees across cities is determined by background climate, urban morphology, and tree traits," *Commun Earth Environ*, vol. 5, p. 754, 2024, doi: 10.1038/s43247-024-01908-4.

[24] S. A. Shiflett, L. L. Liang, S. M. Crum, G. L. Feyisa, J. Wang, and G. D. Jenerette, "Variation in the relationship between urban vegetation and surface temperature across climatic and ecological contexts," *Environmental Research Letters*, vol. 12, no. 12, p. 124007, 2017, doi: 10.1088/1748-9326/aa9f88.

[25] Y. Su *et al.*, "Asymmetric influence of forest cover gain and loss on land surface temperature," *Nature Climate Change 2023 13:8*, vol. 13, no. 8, pp. 823–831, Aug. 2023, doi: 10.1038/s41558-023-01757-7.

[26] L. Zhu *et al.*, "Comparable biophysical and biogeochemical feedbacks on warming from tropical moist forest degradation," *Nature Geoscience 2023 16:3*, vol. 16, no. 3, pp. 244–249, Mar. 2023, doi: 10.1038/s41561-023-01137-y.

[27] I. Agathangelidis, G. Blougouras, C. Cartalis, A. Polydoros, C. G. Tzanis, and K. Philippopoulos, "Global climatology of the daytime surface cooling of urban parks using satellite observations," *Geophys Res Lett*, vol. 52, no. 4, p. e2024GL112887, 2025, doi: 10.1029/2024GL112887.

[28] X. Cao, A. Onishi, J. Chen, and H. Imura, "Quantifying the cool island intensity of urban parks using ASTER and IKONOS data," *Landsc Urban Plan*, vol. 96, no. 4, pp. 224–231, 2010, doi: 10.1016/j.landurbplan.2010.03.008.

[29] S. Guha, H. Govil, and A. Dey, "Examining the relationship between land surface temperature and multiple vegetation indices in Delhi, India," *Spatial Information Research*, vol. 29, no. 5, pp. 667–682, 2021, doi: 10.1007/s41324-021-00395-3.

[30] P. K. Cheung, S. J. Livesley, and K. A. Nice, "Estimating the cooling potential of irrigating green spaces in 100 global cities with arid, temperate or continental climates," *Sustain Cities Soc*, vol. 71, p. 102974, 2021, doi: 10.1016/j.scs.2021.102974.

[31] "Urban Atlas: Vector Land Cover Data," Copernicus Land Monitoring Service (European Environment Agency), 2018. doi: 10.2909/047f71ee-dec6-4c7b-8044-7a153c025588.

[32] "European Environment Agency (EEA)" CORINE Land Cover, "CORINE Land Cover 2018 – Technical Guidelines," 2018. [Online]. Available: https://land.copernicus.eu/en/technical-library/clc-2018-technical-guidelines

[33] J. P. Walawender, M. Szymanowski, M. J. Hajto, and A. Bokwa, "Land surface temperature patterns in the urban agglomeration of Kraków (Poland) derived from Landsat-7/ETM+ data," *Pure Appl Geophys*, vol. 171, no. 6, pp. 913–940, 2014, doi: 10.1007/s00024-013-0685-7.

[34] D. Bates, M. Mächler, B. Bolker, and S. Walker, "Fitting Linear Mixed-Effects Models Using lme4," *J Stat Softw*, vol. 67, no. 1, pp. 1–48, 2015, doi: 10.18637/jss.v067.i01.

[35] J. C. Pinheiro and D. M. Bates, *Mixed-Effects Models in S and S-PLUS*. New York, NY: Springer, 2000. doi: 10.1007/b98882.

[36] B. M. Bolker *et al.*, "Generalized linear mixed models: a practical guide for ecology and evolution," *Trends Ecol Evol*, vol. 24, no. 3, pp. 127–135, 2009, doi: 10.1016/j.tree.2008.10.008.

[37] A. Kuznetsova, P. B. Brockhoff, and R. H. B. Christensen, "lmerTest Package: Tests in Linear

Mixed Effects Models," *J Stat Softw*, vol. 82, no. 13, pp. 1–26, 2017, doi: 10.18637/jss.v082.i13.

[38] C. J. Tucker, "Red and photographic infrared linear combinations for monitoring vegetation," *Remote Sens Environ*, vol. 8, no. 2, pp. 127–150, 1979.

[39] B.-C. Gao, "NDWI—A normalized difference water index for remote sensing of vegetation liquid water from space," *Remote Sens Environ*, vol. 58, no. 3, pp. 257–266, 1996, doi: 10.1016/S0034-4257(96)00067-3.

[40] Y. Song, H. Xu, T. Liu, J. Xu, and X. Song, "Linking spatiotemporal variations in urban land surface temperature to land use and land cover: A case study in Hangzhou City, China," 2024. doi: 10.2139/ssrn.5027000.

[41] USGS, "Landsat 4–7 Collection 2 Level-2 Science Products Guide," 2021. Accessed: Aug. 26, 2025. [Online]. Available: https://www.usgs.gov/media/files/landsat-4-7-collection-2-level-2-science-product-guide

[42] USGS, "Landsat 8–9 Collection 2 Level-2 Surface Temperature (ST) Product Guide," 2021. [Online]. Available: https://www.usgs.gov/media/files/landsat-8-9-collection-2-level-2-science-product-guide

[43] H. Schielzeth, "Simple means to improve the interpretability of regression coefficients," *Methods Ecol Evol*, vol. 1, no. 2, pp. 103–113, 2010, doi: 10.1111/j.2041-210X.2010.00012.x.

[44] S. Nakagawa and H. Schielzeth, "A General and Simple Method for Obtaining R2 from Generalized Linear Mixed-Effects Models," *Methods Ecol. Evol*, vol. 4, no. 2, pp. 133–142, 2012, doi: 10.1111/j.2041-210X.2012.00261.x.

[45] S. Nakagawa, P. C. D. Johnson, and H. Schielzeth, "The coefficient of determination R^2 and ICC from GLMMs revisited and expanded," *J R Soc Interface*, vol. 14, p. 20170213, 2017, doi: 10.1098/rsif.2017.0213.

[46] J. Fox and S. Weisberg, *An R Companion to Applied Regression*, 3rd ed. Thousand Oaks, CA: SAGE Publications, Inc., 2019.

[47] P. A. P. Moran, "Notes on continuous stochastic phenomena," *Biometrika*, vol. 37, no. 1–2, pp. 17–23, 1950, doi: 10.1093/biomet/37.1-2.17.

[48] D. Li, T. Chakraborty, J. Yang, L. Zhou, M. R. Kaloop, and A. Hsu, "Clear-sky bias in satellite-derived SUHI intensities," *Geophys Res Lett*, vol. 50, p. e2022GL101492, 2023, doi: 10.1029/2022GL101492.

[49] R. A. Spronken-Smith and T. R. Oke, "The thermal regime of urban parks in two cities with different summer climates," *Int J Remote Sens*, vol. 19, no. 11, pp. 2085–2104, 1998.

[50] X. Guan, Y. Li, J. M. Chen, Y. Ma, and H. Shen, "A process model-guided transfer learning framework for mapping global gross primary production," *Agric For Meteorol*, vol. 372, p. 110678, Sep. 2025, doi: 10.1016/J.AGRFORMET.2025.110678.

[51] J. Tan, D. Yu, Q. Li, X. Tan, and W. Zhou, "Spatial relationship between land-use/land-cover change and land surface temperature in the Dongting Lake area, China," *Sci Rep*, vol. 10, p. 9245, 2020, doi: 10.1038/s41598-020-66168-6.

[52] H. Shen, Y. Ran, X. Guan, D. Chu, and D. Li, "A Parameter and Flag Adaptive Reconstruction Method for Satellite Vegetation Index Time Series," *IEEE Transactions on Geoscience and Remote Sensing*, vol. 63, 2025, doi: 10.1109/TGRS.2025.3568444.

[53] J. Li, X. Liu, Y. Li, and M. Liu, "Combining Filling and Fusion Strategies for Generating Synthetic Daily Landsat Time Series Image on Google Earth Engine," *IEEE Transactions on Geoscience and Remote Sensing*, vol. 63, 2025, doi: 10.1109/TGRS.2025.3531890.

[54] X. Guan *et al.*, "Fusing MODIS and AVHRR products to generate a global 1-km continuous NDVI time series covering four decades," *Big Earth Data*, vol. 9, no. 1, pp. 72–99, Jan. 2025, doi: 10.1080/20964471.2024.2448072.